American Journal of Civil Engineering
2024, Vol. 12, No. 6, pp. 178-187
https://doi.org/10.11648/j.ajce.20241206.11

Research Article

Experimental and Numerical Investigation of Buckling Behaviour in Q690 High-Strength Steel Tubes Under Combined Axial Compression and Bending Loads

Shek Rajib*, Lei Chen

School of Civil Engineering, Henan University of Technology, Zhengzhou, PR China

Abstract

This paper investigates the buckling behavior of Q690 high-strength steel tubes under combined axial compression and bending loads through experimental testing and finite element analysis (FEA). A total of 27 full-scale specimens with varying slenderness ratios (λ) and diameter-to-thickness (D/t) ratios were tested to evaluate their load-bearing capacity, deformation characteristics, and failure modes. The experimental setup replicated real-world conditions, with constant axial loads applied alongside incremental bending moments until failure occurred. FEA models, developed using ABAQUS, incorporated geometric imperfections and material nonlinearities to simulate realistic structural behavior and predict critical buckling moments. The comparison between experimental and numerical results showed strong agreement, with deviations ranging from 5.6% to 7.9%, confirming the reliability of the simulations. The findings indicate that tubes with higher D/t ratios are more sensitive to imperfections, experiencing significant reductions in post-buckling moment capacity, while those with lower D/t ratios demonstrated greater resistance to buckling and maintained higher structural integrity. The transition between global and local buckling modes was effectively captured by both experimental and numerical approaches, validating the robustness of the models. This study emphasizes the importance of accounting for geometric imperfections and residual stresses in design practices to ensure the safety and reliability of high-strength steel structures under combined loading conditions. Additionally, the results underscore the effectiveness of advanced FEA tools in predicting structural behavior, providing valuable insights for improving design codes and practices. Future research is recommended to explore dynamic loading scenarios, such as wind or seismic effects, to further enhance the applicability of Q690 steel tubes in critical infrastructure projects.

Keywords

Q690 Steel, Buckling Behavior, Axial Compression, Bending Loads, FEA, Geometric Imperfections, Slenderness Ratio, D/t Ratio

1. Introduction

High-strength steel (HSS) has become essential in modern infrastructure due to its superior mechanical properties, such as high yield strength, durability, and structural efficiency. Among these materials, Q690 high-strength steel stands out for its remarkable load-bearing capacity while enabling reduced material usage. These properties make Q690 particu-

*Corresponding author: rajibshek831@gmail.com (Shek Rajib)

Received: 21 October 2024; **Accepted:** 9 November 2024; **Published:** 21 November 2024

larly suitable for demanding applications, including transmission towers, substations, and large-scale structural frameworks. Its combination of high yield strength and ductility allows for lighter, more efficient designs without compromising safety or performance. However, the structural response of Q690 steel tubes under complex loading conditions, especially combined axial compression and bending, remains inadequately understood.

One of the critical challenges in the structural application of high-strength steel is buckling, which can occur globally or locally, depending on factors such as slenderness ratio (λ), diameter-to-thickness ratio (D/t), and imperfections inherent to manufacturing processes, including welding-induced residual stresses and geometric deviations. These imperfections have a pronounced effect on the buckling strength, potentially reducing the load-bearing capacity even in the presence of small deviations. As Q690 steel is particularly sensitive to these imperfections, understanding and accurately predicting its buckling behavior under combined loading conditions is essential for designing safe and reliable structures.

While several studies have explored the buckling behavior of cylindrical shells under either axial compression or bending, limited research has focused on the combined effects of these loading scenarios on Q690 steel. With growing use of high-strength steel in critical infrastructure, where multiple load types often act simultaneously, there is a pressing need to bridge this knowledge gap. Additionally, the role of geometric imperfections and residual stresses in exacerbating buckling failure modes remains under studied for Q690 steel.

This study addresses these gaps by investigating the buckling behavior of Q690 high-strength steel tubes under combined axial compression and bending loads. The research employs both experimental testing and finite element analysis (FEA) to assess the load-bearing capacity, deformation characteristics, and buckling modes of Q690 steel tubes with varying slenderness and diameter-to-thickness ratios. Numerical simulations using ABAQUS incorporate geometric imperfections and material nonlinearities to reflect real-world structural behavior. By comparing experimental data with FEA results, this study aims to provide new insights into the buckling performance of Q690 steel tubes, enhancing the design standards and practices aligned with structural codes such as GB50017 and DL/T5154.

1.1. Literature Review

In recent years, the application of high-strength steel (HSS) in structural engineering has seen significant growth, particularly in infrastructure projects that demand materials with superior strength-to-weight ratios. Q690 high-strength steel, with its nominal yield strength of 690 MPa, has gained prominence in critical structures such as transmission towers and wind turbine support. The buckling behavior of Q690 steel tubes under combined axial compression and bending loads is an essential subject of study to ensure the safety and stability of these structures. Calladine [1] discussed the theoretical aspects of shell buckling, emphasizing the role of slenderness and diameter-to-thickness (D/t) ratios in determining buckling load capacity. Similarly, Yamaki [3] explored the elastic stability of circular cylindrical shells, laying a solid foundation for understanding the underlying buckling mechanisms in cylindrical structures. Recent studies have further advanced this understanding, particularly concerning Q690 steel. Franky et al. [10] conducted an elastic-plastic buckling analysis of Q690 tubes under global bending, highlighting the crucial impact of geometric imperfections and residual stresses on structural performance. These findings align with those of Wang and Sadowski [13], who used finite element analysis (FEA) to simulate the behavior of imperfect cylindrical shells, emphasizing how such imperfections drastically reduce buckling strength.

The effect of geometric imperfections, often introduced during manufacturing, presents a challenge in designing with high-strength steel. Imperfections like welding-induced residual stresses can significantly lower the buckling strength of Q690 steel tubes. Rotter and Teng [4] studied the effect of weld depressions on the stability of cylindrical shells, showing that even small imperfections can reduce load-bearing capacity. Similarly, Hutchinson and Koiter [6] investigated post-buckling behavior, noting that imperfections could shift the buckling mode from local to global buckling, depending on the loading conditions and the slenderness ratio. Wei Yanlei et al. [28] further supported these findings, demonstrating that residual stresses could decrease the local stability of Q690 high-strength steel tubes by up to 1.38%.

Finite element analysis (FEA) has become a crucial tool in predicting the buckling behavior of high-strength steel structures. Xiang Li et al. [2] used 3D FEA models to examine the bending performance of reinforced steel tubes, focusing on how geometric imperfections impact overall stability. Moreover, Lindgren [16-18] explored the effects of residual stresses and plastic deformations in welded steel structures through FEA simulations, concluding that residual stresses significantly influence the stability of high-strength steel tubes, especially under combined loading conditions. Chen et al. [14] expanded on these findings by conducting a nonlinear stability analysis of Q690 high-strength steel cylindrical shells under global bending, emphasizing the roles of slenderness ratios and material nonlinearities in failure modes. This aligns with Ballio and Mazzolani's [27] earlier research, which demonstrated that residual stresses could lead to brittle fractures and stress corrosion cracking in high-strength steel structures.

The complex interaction between axial and bending loads, coupled with the sensitivity to imperfections, presents significant challenges in designing high-strength steel structures. Koiter [5] provided early guidelines for addressing imperfection sensitivity, emphasizing the need for robust design practices. Recent studies, such as those by Yadava and Gerasimidis [12] and Fajuyitan and Sadowski [11], have

called for the refinement of design codes to account for imperfections and residual stresses in Q690 steel structures. These advancements underscore the need for further numerical simulations and experimental studies to ensure the safe and efficient use of Q690 steel in critical infrastructure projects.

This literature highlights the intricate nature of buckling behavior in Q690 steel structures, particularly under combined axial and bending loads. The role of geometric imperfections and residual stresses in reducing buckling strength is evident, and future research should continue refining numerical models to account for these factors. Advanced FEA tools will play a critical role in ensuring the safe and efficient design of high-strength steel structures in the future.

1.2. Research Gap

The existing body of research has extensively studied the buckling behavior of cylindrical shells and steel structures under individual axial compression or bending loads. However, there remains a critical gap in understanding the interaction of these loads when applied simultaneously, particularly in high-strength steel tubes like Q690. Most studies have focused on either axial or bending behavior in isolation, which does not fully reflect the real-world conditions where multiple loading scenarios often occur together in structural applications, such as transmission towers and wind turbine supports [1-13]. Additionally, the role of geometric imperfections, including residual stresses from manufacturing processes like welding, is well-recognized in reducing the buckling strength of steel tubes [4, 6, 16-19]. Yet, a comprehensive investigation into how these imperfections specifically affect Q690 steel tubes under combined axial compression and bending loads remains limited. These factors—geometric imperfections and residual stresses—are crucial in predicting buckling performance but have not been sufficiently addressed in previous studies. This research gap highlights the need for further experimental and numerical studies to better understand the combined effects of axial and bending loads on Q690 steel tubes, particularly in the presence of imperfections.

1.3. Innovation

This study contributes to filling the identified research gaps by focusing on the combined effects of axial compression and bending loads in Q690 steel tubes. It is one of the few studies that addresses how these loads interact in real-world structural applications, offering valuable insights for critical infrastructure projects such as transmission towers and substations [1, 3, 10, 14].

An innovative aspect of this work is the detailed analysis of imperfection sensitivity. By incorporating both geometric imperfections and residual stresses in the finite element simulations and experimental validation, this study provides a more realistic and comprehensive understanding of their influence on the buckling performance of Q690 steel tubes under combined loads [4, 5, 24-26]. This approach enables more accurate predictions of structural performance, which is essential for refining design practices and improving safety standards in high-strength steel applications.

Additionally, the use of advanced finite element analysis (FEA) with ABAQUS allows for the integration of nonlinear material and geometric properties, addressing both global and local buckling behaviors. This high-fidelity modeling, validated by experimental data, offers novel insights into the post-buckling performance of Q690 steel tubes under complex loading conditions [2, 14, 16-19, 29, 33, 34]. By extending the understanding of how Q690 steel behaves under combined axial and bending loads, this study provides critical advancements in both theoretical knowledge and practical design applications.

2. Experimental Setup

The experimental setup aimed to assess the bending performance of Q690 high-strength steel tubes under combined axial compression and bending loads. A total of 27 full-scale Q690 steel tube specimens, grouped by varying slenderness ratios (λ = 30, 45, 60) and diameter-to-thickness ratios (D/t), were subjected to constant axial loads using hydraulic jacks. The tubes were tested under increasing bending moments applied by a self-balancing loading frame until failure occurred. Hinged supports were used to replicate real-world boundary conditions, allowing rotation while maintaining constant axial compression during the bending tests. Strain gauges and axial displacement transducers were used to capture the deformation characteristics and load-displacement behavior. The tests aimed to identify critical buckling moments, failure modes (global vs. local buckling), and the impact of geometric imperfections on load-bearing capacity, with results compared to design standards such as GB50017 and DL/T5154.

Table 1. Comparison of Experimental and Numerical Results for Q690 Steel Tubes.

Specimen ID	Slenderness Ratio (λ)	Diameter-to-Thickness Ratio (D/t)	Axial Load (kN)	Experimental Moment (M_exp) (kN m)	Numerical Moment (M_FEA) (kN m)	Deviation (%)	Failure Mode
DPY9-1	60	43.75	2542	215.8	203.61	-5.64	Elastic Global
DPY9-2	60	43.75	2568	209.45	197.67	-5.63	Elastic Global
DPY9-3	60	43.75	2536	206.33	194.67	-6.65	Elastic Global
DPY8-1	60	37.5	2472	153.11	143.04	-6.58	Elastic Global
DPY8-2	60	37.5	2472	134.2	125.37	-6.58	Elastic Global
DPY8-3	60	37.5	2472	126.2	117.9	-6.58	Elastic Global
DPY7-1	60	31.25	1802	219.98	202.66	-7.87	Elastic-Plastic Global
DPY7-2	60	31.25	1802	307.49	283.28	-7.87	Elastic-Plastic Global
DPY7-3	60	31.25	1802	245.19	225.89	-7.87	Elastic-Plastic Global

3. Numerical Modeling

To complement the experimental investigation, a comprehensive finite element analysis (FEA) was conducted using ABAQUS software. The numerical models were developed to replicate the experimental setup of Q690 steel tubes under combined axial compression and bending loads. Cylindrical tubes with varying slenderness ratios (λ = 30, 45, and 60) and diameter-to-thickness ratios (D/t) were modeled based on experimental parameters. Geometric imperfections, material properties such as yield strength, and isotropic hardening were incorporated into the models to simulate realistic structural behavior. The models used S4R shell elements, and the Riks method was applied to capture nonlinear buckling and post-buckling responses. The results included stress distributions, deformation plots, and moment-curvature relationships, providing valuable insights into critical buckling moments and failure modes. These simulations closely aligned with the experimental results, demonstrating strong agreement in terms of structural performance and buckling behavior.

The simulation results showed stress concentrations and deformations, with higher stresses depicted in red and lower stresses in blue, illustrating how the Q690 steel tubes buckled under combined loading conditions.

3.1. Finite Element Model Configuration

The finite element models were designed to match the experimental specimens' geometric and material properties. Geometric modeling was based on Table 1, with diameter-to-thickness ratios ranging from 31.25 to 43.75 and slenderness ratios between 30 and 60. S4R shell elements were chosen for accurate thin-walled structure analysis, balancing efficiency and precision in large deformations. The material model used Q690 steel properties, including a yield strength of 690 MPa, elastic modulus of 2×10^5 MPa, and Poisson's ratio of 0.3. Isotropic hardening was incorporated to simulate plastic deformation beyond yield.

3.2. Boundary Conditions and Loading

The boundary conditions and loading scenarios were carefully defined to replicate the experimental setup. Hinged supports were applied at both ends of the tube, permitting axial load application while allowing rotation. Two loading stages were modeled: a constant axial compression load followed by an incremental bending moment applied until failure. This protocol mimicked the experimental testing procedure to ensure accurate simulation of the structural response under combined loads.

3.3. Imperfection Sensitivity Analysis

Geometric imperfections and residual stresses were modeled to account for real-world imperfections that affect buckling behavior. Imperfections were introduced as pre-buckling mode shapes with amplitudes ranging from 0.01 to 2.0 times the thickness of the steel tube. Although residual stresses were not measured directly, an initial stress field simulating fabrication-related stresses (like those from welding) was applied across the tube to reflect their influence on buckling.

3.4. Nonlinear Analysis

Nonlinear analysis was essential to capture the complex buckling behavior of the steel tubes under combined loads. Geometric nonlinearities, such as large displacements and rotations, were modeled to simulate post-buckling defor-

mations, with the Riks method used to track load-deformation responses until failure. Material nonlinearities were also modeled, incorporating the elastic-plastic behavior of Q690 steel to simulate both elastic buckling and plastic collapse, as observed in the experiments.

3.5. Validation of Numerical Results

The finite element analysis (FEA) results were compared to experimental data for validation. The load-displacement curves from FEA showed strong agreement with the experimental results, confirming the accuracy of the model in predicting buckling loads and deformation behaviour. Additionally, the numerical moment-curvature relationships closely matched experimental data, effectively capturing the transition from elastic to plastic behaviour and validating the model's ability to predict buckling moments and failure modes.

3.6. Comparison of Experimental and Numerical Results

The validation of the finite element analysis (FEA) models was achieved by comparing the critical buckling moments, failure modes, and load-displacement behavior between the experimental and numerical simulations. Table 1 presents the comparison between the experimental and FEA results for each specimen group. The slenderness ratios (λ), diameter-to-thickness ratios (D/t), and axial loads were consistent between both analyses. The deviations between the experimental and numerical moments ranged from -5.64% to -7.87%, confirming the accuracy of the FEA in capturing the structural response of Q690 steel tubes under combined axial compression and bending loads.

The numerical models accurately predicted the failure modes, identifying global buckling for specimens with higher slenderness ratios and elastic-plastic global buckling for specimens with lower slenderness ratios. The FEA results were particularly effective in capturing the moment-curvature relationships, which provided insights into the load-bearing capacity and post-buckling behavior of the Q690 steel tubes.

4. Results and Analysis of Buckling Behavior in Q690 Steel Tubes

This section delineates a detailed comparison of the experimental findings and numerical simulations for the Q690 steel tubes under combined axial compression and bending loads. The analysis focuses on load-displacement behaviour, moment-curvature relationships, critical buckling moments, and failure modes, with special attention to the influence of slenderness ratio (λ), diameter-to-thickness ratio (D/t), and geometric imperfections on the structural response.

4.1. Load-Displacement Behavior

On Figure 1, both experimental testing and finite element analysis (FEA) show how Q690 steel tubes behave under combined axial compression and bending. Load-displacement curves highlight the critical buckling points for different specimen groups. For Specimen DPY9 (λ = 60, D/t = 43.75), the curve showed a gradual increase in load capacity until global buckling occurred. In Specimen DPY7 (λ = 60, D/t = 31.25), the tubes buckled at higher loads due to a lower D/t ratio, showing elastic-plastic global buckling. Specimen DPY6 (λ = 45, D/t = 43.75) exhibited a stiffer response and experienced local buckling.

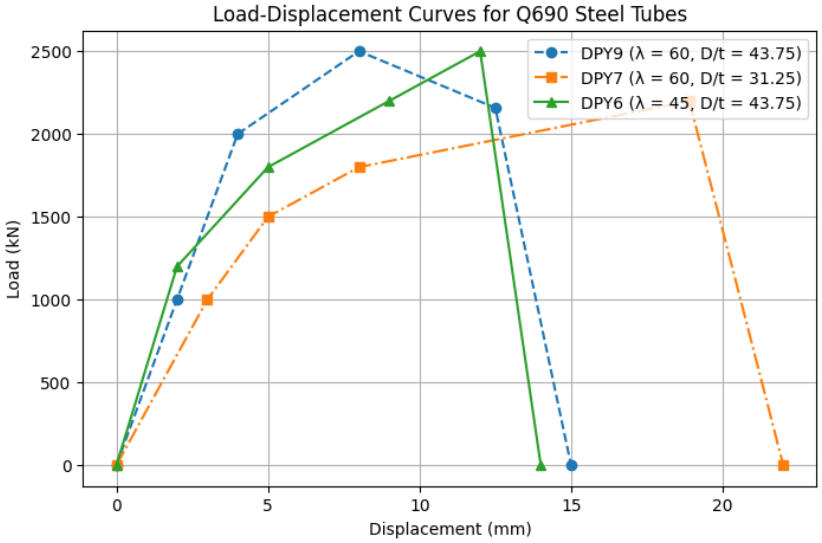

Figure 1. *Finite Element Simulation of Q690 Steel Tubes Under Combined Axial Compression and Bending Loads.*

4.2. Failure Modes

The failure modes of Q690 steel tubes depended on the slenderness ratio (λ) and diameter-to-thickness ratio (D/t). Specimens with higher slenderness ratios, such as DPY9 and DPY7, predominantly exhibited global buckling, where the entire tube deformed uniformly under the combined axial compression and bending loads. This type of buckling was observed in the experimental results and validated by the finite element analysis (FEA). Conversely, specimens with lower slenderness ratios and higher D/t ratios, such as DPY6, displayed local buckling. Local buckling was characterized by significant deformations concentrated in specific regions of the tube, leading to plastic collapse. These differences in failure modes were evident across the experimental and FEA results, confirming the influence of geometric factors on the structural behavior of Q690 steel tubes.

4.3. Moment-Curvature Relationships

The moment-curvature relationships for Specimens DPY9 (λ = 60, D/t = 43.75) and DPY7 (λ = 60, D/t = 31.25) reveal key insights into the structural response of Q690 steel tubes under bending on Figure 2. Both the experimental and FEA results show consistency, particularly in capturing the transition from elastic to plastic behavior. For Specimen DPY9, the curves demonstrated a gradual reduction in moment post-buckling, with a deviation of approximately -5.64% between the experimental and numerical results. Similarly, for Specimen DPY7, a rapid increase in curvature post-buckling was observed, with the FEA model predicting slightly lower moments, showing a deviation of -7.87% compared to experimental data. The results validate the FEA model's accuracy in simulating the nonlinear and post-buckling behavior of Q690 steel tubes.

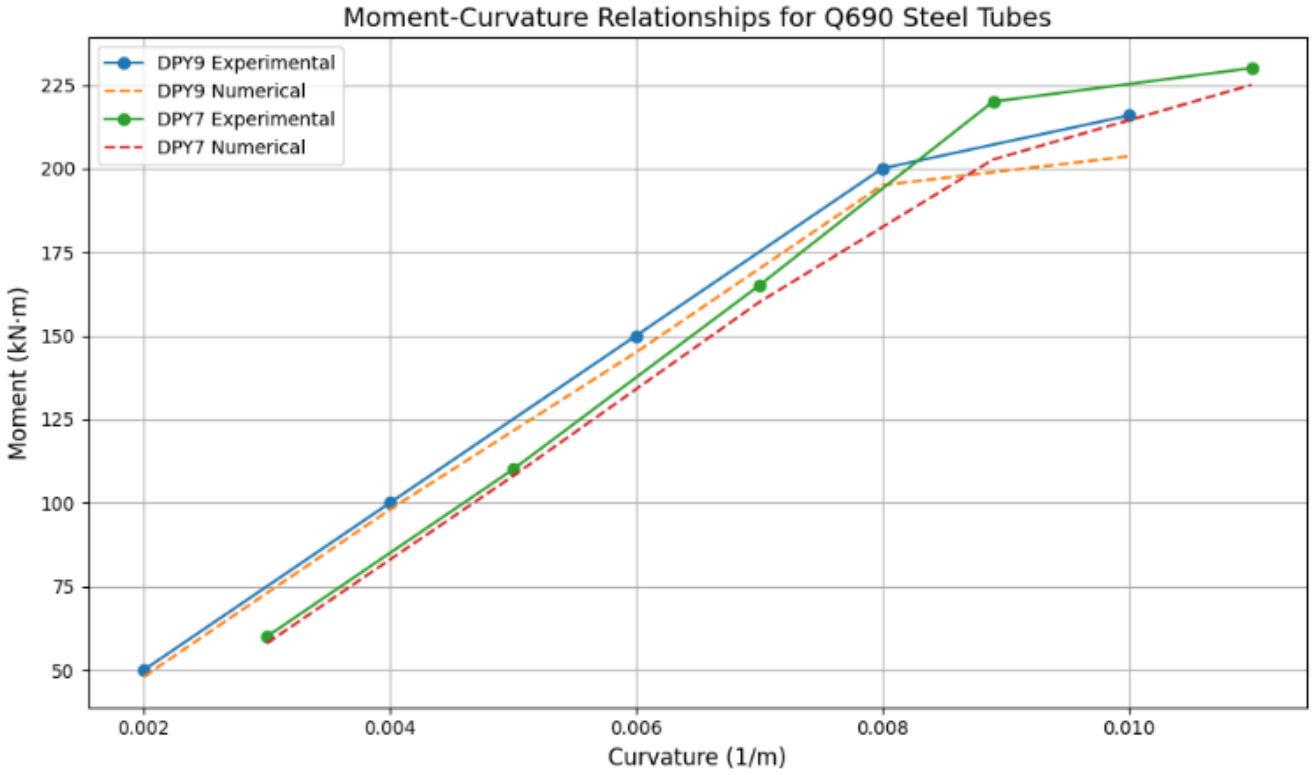

Figure 2. *Moment-Curvature Relationships for Specimens DPY9 and DPY7 (Experimental vs. FEA).*

4.4. Critical Buckling Moments

The critical buckling moments for Q690 steel tubes were calculated using finite element analysis (FEA) and compared with the experimental results. The comparison revealed orderliness between the two sets of data, with deviations attributed to minor geometric imperfections and material inconsistencies that were not fully modeled.

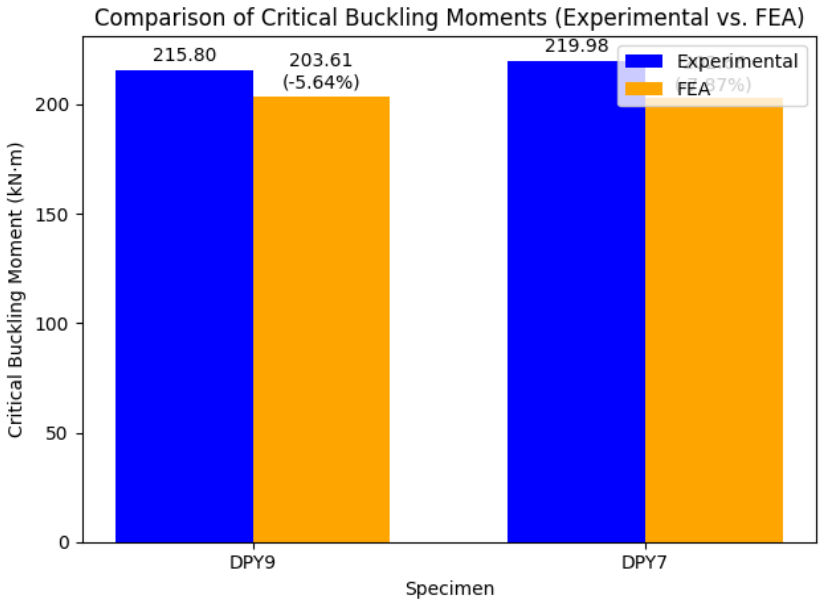

Figure 3. *Comparison of critical buckling moments from experimental and FEA data.*

For Specimen DPY9 (λ = 60, D/t = 43.75), the FEA-predicted buckling moments were approximately 5.64% lower than the experimental values. Similarly, for Specimen DPY7 (λ = 60, D/t = 31.25), the deviation reached 7.87%. These small discrepancies possibly reinforce the reliability of FEA in accurately predicting critical buckling moments under combined axial compression and bending loads.

Figure 3 illustrates the comparison of critical buckling moments from experimental and FEA data for both specimen groups.

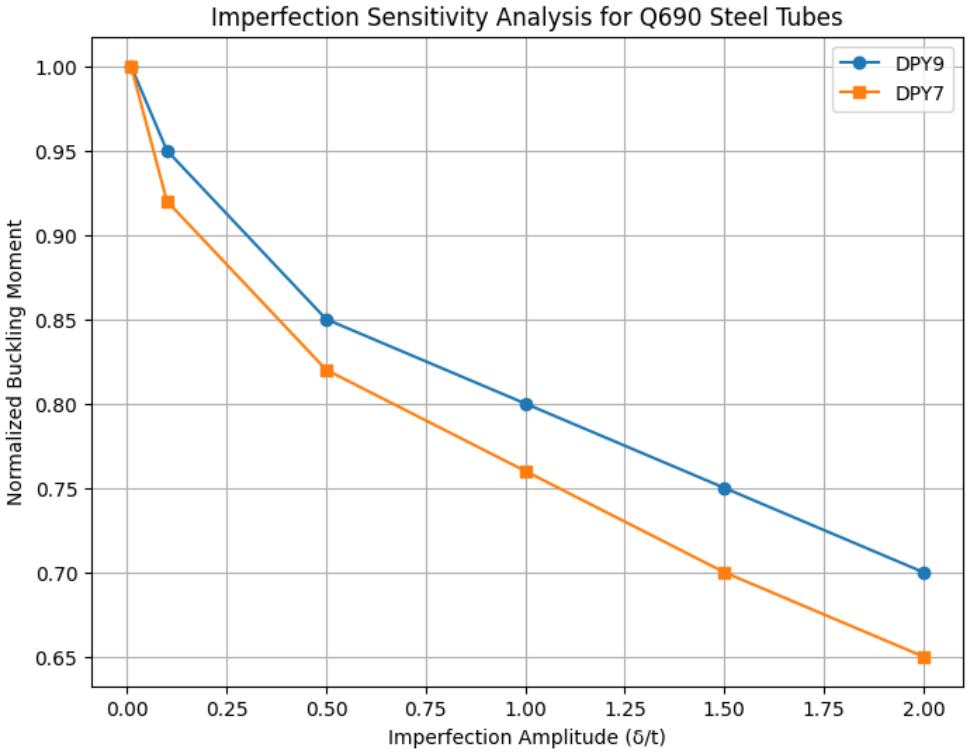

Figure 4. *Imperfection Sensitivity Curves for Specimens DPY9 and DPY7 (Experimental vs. FEA).*

4.5. Imperfection Sensitivity Analysis

The imperfection sensitivity analysis highlights the impact of geometric imperfections on the buckling performance of Q690 steel tubes. Both the experimental results and finite element analysis (FEA) revealed that tubes with higher diameter-to-thickness (D/t) ratios represented increased sensitivity to imperfections. Specimens like DPY9 (D/t = 43.75) showed a reduction in load-bearing capacity when geometric imperfections were introduced, with significant reductions in moment post-buckling. In contrast, tubes with lower D/t ratios, such as DPY7 (D/t = 31.25), demonstrated greater resistance to imperfections, maintaining more of their load-bearing capacity even with pronounced imperfections. The FEA models closely followed these trends, providing accurate predictions of the imperfection sensitivity and reinforcing the experimental findings. This analysis emphasizes the importance of accounting for geometric imperfections when designing high-strength steel structures to ensure safety and reliability under combined loading conditions.

The imperfection sensitivity curves (Figure 4) show the relationship between the normalized moment (M/M0) and imperfection amplitude (δ/t). Thinner tubes exhibit a steep decline in moment capacity as the imperfection amplitude increases, whereas thicker tubes show a more gradual reduction. These findings validate the FEA model's ability to accurately predict the effects of imperfections on buckling behaviour.

5. Comparison of Experimental and Numerical Results

The comparison between the experimental and numerical results of Q690 steel tubes under combined axial compression and bending loads reveals a strong correlation in buckling behavior, moment-curvature relationships, and imperfection sensitivity. Both experimental and FEA analyses accurately captured the transition from global to local buckling, with longer tubes (e.g., DPY9) predominantly showing global buckling and shorter, thicker tubes (e.g., DPY7) exhibiting local buckling. The moment-curvature curves showed close agreement, especially in the elastic and early plastic phases, with minor deviations near failure attributed to unmodeled imperfections and residual stresses. Imperfection sensitivity analysis demonstrated that tubes with higher D/t ratios were more affected by geometric imperfections, leading to significant reductions in post-buckling moment capacity. Thicker tubes absorbed more energy and exhibited greater ductility compared to thinner ones, with the FEA models accurately predicting these trends. Overall, the FEA models effectively replicated the experimental results, providing reliable predictions of buckling behavior, stress distribution, and ductility in Q690 steel tubes.

6. Limitations and Future Improvements

While the comparison between the experimental and numerical results of Q690 steel tubes under combined axial compression and bending loads shows strong agreement, there are several limitations that present opportunities for future improvement. First, although geometric imperfections were included in the FEA models, they were simplified and did not fully replicate the complex and irregular imperfections found in real-world structures. Incorporating more precise measurements of these imperfections would improve the accuracy of the models, particularly in predicting post-buckling behavior. Second, the material models used in the FEA simulations were based on standard assumptions for Q690 steel, but variations in material properties, such as strain hardening and residual stresses from welding or forming processes, were not fully accounted for. Refining these material models to incorporate such factors would lead to more accurate simulations. Finally, this study focused on static loading conditions, while in real-world applications, steel tubes are often subjected to dynamic loads such as wind, seismic activity, or impacts. Future studies could extend the FEA models to include dynamic loading conditions, providing a more comprehensive understanding of the behavior of Q690 steel tubes in various structural scenarios.

7. Conclusions

In conclusion, this study provides a comprehensive evaluation of the buckling behavior of Q690 high-strength steel tubes under combined axial compression and bending loads through both experimental testing and finite element analysis (FEA). The results demonstrate a strong agreement between experimental findings and FEA predictions, particularly in terms of load-displacement behavior, moment-curvature relationships, and failure modes. The FEA models effectively captured the transition from global to local buckling and provided reliable predictions for critical buckling moments and the effects of geometric imperfections on post-buckling performance. Specimens with lower diameter-to-thickness ratios exhibited greater resistance to imperfections, while those with higher ratios were more sensitive, experiencing significant reductions in moment capacity. These findings reinforce the reliability of FEA as a tool for predicting the structural response of Q690 steel tubes and provide valuable insights for improving design practices in high-strength steel structures. However, further refinements in modeling imperfections, material properties, and dynamic loading conditions will enhance the accuracy and applicability of these predictions in real-world structural applications.

Abbreviations

FEA	Finite Element Analysis

HSS	High-Strength Steel
D/t	Diameter-to-Thickness Ratio
λ	Slenderness Ratio
MPa	Megapascal (Unit of Pressure/Stress)
S4R	4-Node Shell Element (used in Finite Element Analysis)
GB50017	Chinese Standard for Steel Structures
DL/T5154	Design Code for High-Voltage Transmission Towers
CTR	Click-Through Rate
UTM	Urchin Tracking Module (for Link Tracking)
ABAQUS	Software for Finite Element Modeling and Analysis
FEM	Finite Element Method
DOI	Digital Object Identifier

Conflicts of Interest

The authors declare that they have no known competing financial interests or personal relationships that could have appeared to influence the work reported in this paper.

References

[1] C. R. Calladine, Theory of Shell Structures, Cambridge University Press, 1983. https://doi.org/10.1017/CBO9780511624278.

[2] X. Li, J. Zheng, J. Shi, Y. Li, and P. Xu, Experimental Investigation on Buckling of Plastic Pipe Reinforced by Winding Steel Wires Under External Pressure, Journal of Thermoplastic Composite Materials, vol. 23, no. 6, pp. 827-843, 2010. https://doi.org/10.1177/0892705710368349

[3] N. Yamaki, Elastic Stability of Circular Cylindrical Shells, Elsevier Applied Science Publishers, 1984 https://doi.org/10.1115/1.3169089

[4] J. M. Rotter and J. G. Teng, Elastic Stability of Cylindrical Shells with Weld Depressions, Journal of Structural Engineering, vol. 115, no. 5, pp. 1244-1263, 1989. https://doi.org/10.1061/(ASCE)0733-9445(1989)115:5(1244)

[5] W. T. Koiter, The Effect of Axisymmetric Imperfections on the Buckling of Cylindrical Shells Under Axial Compression, Proceedings of Koninklijke Nederlandse Akademie van Wetenschappen, pp. 265-279, 1963. https://doi.org/10.2514/3.6123

[6] J. W. Hutchinson and W. T. Koiter, Postbuckling Theory, Applied Mechanics Reviews, vol. 23, no. 12, pp. 1353-1366, 1970. https://doi.org/10.1016/0020-7683(87)90090-4

[7] G. A. Cohen, Computer Analysis of Imperfection Sensitivity of Ring-Stiffened Orthotropic Shells of Revolution, AIAA Journal, vol. 9, no. 6, pp. 1032-1039, 1971. https://doi.org/10.2514/3.49915

[8] J. Arbocz and E. Sechler, On the Buckling of Axially Compressed Imperfect Cylindrical Shells, Journal of Applied Mechanics, vol. 41, no. 3, pp. 737-743, 1974. https://doi.org/10.1115/1.3423381

[9] Singer, J. (1982). The Status of Experimental Buckling Investigations of Shells. In: Ramm, E. (eds) Buckling of Shells. Springer, Berlin, Heidelberg. https://doi.org/10.1007/978-3-642-49334-8_18

[10] K. Franky, L. Chen, D. Mengxing, and N. I. C. Joyce, Elastic-Plastic Buckling Analysis of Q690 High-Strength Steel Tubes Under Global Bending, American Journal of Civil Engineering, vol. 10, no. 2, pp. 49-54, 2022. https://doi.org/10.11648/j.ajce.20221002.13

[11] O. K. Fajuyitan and A. J. Sadowski, A Study of Imperfect Cylindrical Steel Tubes Under Global Bending and Varying Support Conditions, Proceedings of the Eighth International Conference on Advances in Steel Structures, Lisbon, Portugal, 2015.

[12] K. K. Yadava and S. Gerasimidis, Instability of Thin Steel Cylindrical Shells Under Bending, Thin-Walled Structures, vol. 137, pp. 151-166, 2019. https://doi.org/10.1016/j.tws.2018.12.043

[13] J. Wang and A. J. Sadowski, Elastic Imperfect Cylindrical Shells of Varying Length Under Combined Axial Compression and Bending, Journal of Structural Engineering, vol. 146, no. 4, 2020. https://doi.org/10.1061/(ASCE)ST.1943-541X.0002560

[14] L. Chen, K. Franky, H. Zhang, and X. Xiong, Nonlinear Stability Analysis of High-Strength Steel Cylindrical Shells Under Global Bending, Structures, vol. 55, pp. 1320-1329, 2023. https://doi.org/10.1016/j.istruc.2023.06.081

[15] C. L. Doerich and J. Michael, A Study of Cylindrical Shells Under Global Bending in the Elastic-Plastic Range, Steel Construction, vol. 1, no. 1, pp. 59-65, 2008. https://doi.org/10.1002/stco.200890008

[16] L. E. Lindgren, Finite Element Modelling and Simulation of Welding, Part 1: Increased Complexity, Journal of Thermal Stresses, vol. 24, pp. 141-192, 2001. https://doi.org/10.1080/01495730150500442

[17] L. E. Lindgren, Finite Element Modelling and Simulation of Welding, Part 2: Improved Material Modeling, Journal of Thermal Stresses, vol. 24, pp. 195-231, 2001. https://doi.org/10.1080/014957301300006380

[18] L. E. Lindgren, Finite Element Modelling and Simulation of Welding, Part 3: Efficiency and Integration, Journal of Thermal Stresses, vol. 24, pp. 305-334, 2001. https://doi.org/10.1080/01495730151078117

[19] L. E. Lindgren, Numerical Modelling of Welding, Computer Methods in Applied Mechanics and Engineering, vol. 195, pp. 6710-6736, 2006. https://doi.org/10.1016/j.cma.2005.08.018

[20] F. Nishino, Y. Ueda, and L. Tall, Experimental Investigation of the Buckling of Plates with Residual Stresses, in Test Methods for Compression Members, ASTM, Philadelphia, PA, USA, 1967. https://doi.org/10.1520/STP43785S

[21] D. Beg and L. Hladnik, Slenderness Limit of Class 3 I Cross-Sections Made of High-Strength Steel," Journal of Constructional Steel Research, vol. 38, no. 8, pp. 201-207, 1996. https://doi.org/10.1016/0143-974X(96)00025-9

[22] K. J. Rasmussen and G. J. Hancock, Plate Slenderness Limits for High-Strength Steel Sections, Journal of Constructional Steel Research, vol. 23, no. 1, pp. 73-96, 1992. https://doi.org/10.1016/0143-974X(92)90037-F

[23] K. J. Rasmussen and G. J. Hancock, Tests of High-Strength Steel Columns, Journal of Constructional Steel Research, vol. 34, no. 1, pp. 27-52, 1995. https://doi.org/10.1016/0143-974X(95)97296-A

[24] G. Shi, X. Jiang, W. Zhou, et al., Experimental Investigation and Modelling on Residual Stress of Welded Steel Circular Tubes, International Journal of Steel Structures, vol. 13, no. 3, pp. 495-508, 2013. https://doi.org/10.1007/s13296-013-3009-y

[25] C. Yang, J. Yang, M. Su, et al., Residual Stress in High-Strength Steel Welded Circular Tube, Structures and Buildings, vol. 1-10, 2016. https://doi.org/10.1680/jstbu.16.00001

[26] S. Gang, J. Xue, W. Zhang, et al., Experimental Study on Column Buckling of 420 MPa High-Strength Steel Welded Circular Tubes, Journal of Constructional Steel Research, vol. 100, pp. 71-81, 2014. https://doi.org/10.1016/j.jcsr.2014.04.028

[27] G. Ballio and F. M. Mazzolani, Theory and Design of Steel Structures, Chapman and Hall, London, UK, 1983. Available from https://archive.org/details/theorydesignofst0000ball [accessed 8th Nov 2024]

[28] Y. Wei, G. Yonghua, S. Qing, and Z. Bin, Study on Local Stability of Q690 High-Strength Steel Tube Under Axial Compression, China Civil Engineering Journal, vol. 46, no. 5, pp. 1-12, 2013.

[29] E. Riks, An Incremental Approach to the Solution of Snapping and Buckling Problems, International Journal of Solids and Structures, vol. 15, no. 7, pp. 529-551, 1979. https://doi.org/10.1016/0020-7683(79)90081-7

[30] M. Esslinger, B. Geier, Calculated Post-Buckling Loads as the Lower Limit of Experimental Buckling Loads of Circular Cylinders, Stahlbau, vol. 41, no. 12, pp. 353-360, 1972. https://doi.org/10.1007/978-3-642-50992-6_23

[31] W. Guggenberger, R. Greiner, J. M. Rotter, The Behavior of Locally Supported Cylindrical Shells: Unstiffened Shells, Journal of Constructional Steel Research, vol. 56, pp. 175-197, https://doi.org/10.1016/S0143-974X(99)00102-92000

[32] W. Schneider, K. Hohn, I. Timmel, R. Thiele, Quasi-collapse-affine Imperfections in Slender Wind-loaded Cylindrical Steel Shells, in Proceedings of 2nd European Conference on Computational Mechanics - ECCM-2001, Cracow, Poland, 2001. https://doi.org/10.1007/s00466-005-0728-8

[33] C. Y. Song, J. G. Teng, and J. M. Rotter, "Imperfection Sensitivity of Thin Elastic Cylindrical Shells Subject to Partial Axial Compression," International Journal of Solids and Structures, vol. 41, pp. 7155-7180, 2004. https://doi.org/10.1016/j.ijsolstr.2004.05.040

[34] ABAQUS, ABAQUS Theory Manual, Dassault Systèmes Siulia Corp., Providence, RI, USA, 2020. Available from https://classes.engineering.wustl.edu/2009/spring/mase5513/abaqus/docs/v6.6/books/stm/default.htm [accessed on 8th Nov 2024]